Science of the Total Environment 716 (2020) 137072

Contents lists available at ScienceDirect

Science of the Total Environment

journal homepage: www.elsevier.com/locate/scitotenv

Impacts of projected climate change on runoff in upper reach of Heihe River basin using climate elasticity method and GCMs

Zhanling Li [a,c,*], Qiuju Li [a,c], Jie Wang [a,c], Yaru Feng [a,c], Quanxi Shao [b]

[a] School of Water Resources and Environment, China University of Geosciences, Beijing 100083, PR China
[b] CSIRO Data 61, Private Bag 5, Wembley, WA 6913, Australia
[c] MOE Key Laboratory of Groundwater Circulation and Environmental Evolution, China University of Geosciences (Beijing), Beijing 100083, PR China

HIGHLIGHTS

- Runoff elasticities to P and to T were estimated.
- 18 GCMs' performances were assessed by entropy weighted TOPSIS method.
- 10% and 12% increases in P were projected, producing 5.6% and 6.7% runoff increases.
- 2.0 °C and 2.9 °C increases in T were projected, producing 2.0% and 2.9% runoff decreases.

GRAPHICAL ABSTRACT

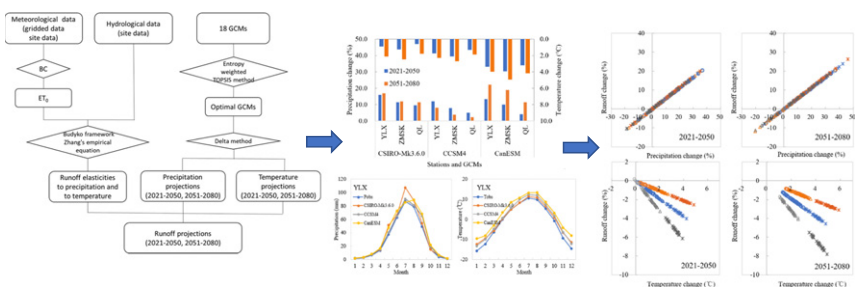

ARTICLE INFO

Article history:
Received 13 June 2019
Received in revised form 30 October 2019
Accepted 31 January 2020
Available online 1 February 2020

Editor: Sangam Shrestha

Keywords:
Budyko
Climate elasticity
GCM
TOPSIS

ABSTRACT

Understanding the impacts of climate change on runoff is of great importance for water resource assessments and adaptation strategy developments especially for the areas where scare and unevenly distributed water are available. Compared to the hydrological modelling method, the climate elasticity method is more flexible with the advantage of using few data in addressing the issue of investigating the effects of climate change on runoff. This study employed Budyko-based climate elasticity method, combined with temperature-based Blaney-Criddle equation, to obtain the elasticities of runoff to two major climate variables, and then applied this methodology to the upper reach of Heihe River basin, China. The runoff elasticity to precipitation in the study area was estimated to be 0.56–0.57, and the elasticity to temperature was −0.017 to −0.018. Precipitation increases showed a positive effect to runoff increases, and temperature increases showed a negative effect. Performances of 18 General Circulation Models (GCMs) of the Coupled Model Intercomparison Project Phase 5 (CMIP5) were assessed and the best GCMs were selected based on the entropy weighted TOPSIS approach. CSIRO-Mk3.6.0, CCSM4, and CanESM2 were ranked the first three with the best performances in simulating the observed precipitation and temperature over the study area. Climate projections from the above three GCMs showed that precipitation increased by 10% and 12% on average during the two periods of 2021–2050 and 2051–2080, producing 5.6% and 6.7% decreases in the projected long-term runoff compared to those in baseline period (1961–1990). Temperatures were projected to be increased by 2.0 °C and 2.9 °C for the two periods, resulting in the future long-term runoff decreased by nearly 2.0% and 2.9%, respectively.

* Corresponding author at: School of Water Resources and Environment, China University of Geosciences, No. 29 Xueyuanlu Road, Haidian District, Beijing 100083, PR China.
E-mail address: zhanling.li@cugb.edu.cn (Z. Li).

https://doi.org/10.1016/j.scitotenv.2020.137072
0048-9697/

1. Introduction

Heihe River basin, the second largest inland river basin in northwestern of China, has a very important strategic position. The middle reach of the basin is in the ancient "Silk Road" and the current Asia-Europe Continental Bridge, and it has become one of the top ten commodity grain bases in China with a long history of agriculture; the Ejina Oasis in the lower reach is an important ecological security barrier (Wang et al., 2019). Thus, water resources in the basin undoubtedly play a vital role in developing irrigation in the middle reach and maintaining a healthy and sustainable oasis system in the lower reach. However, the water resource availability is limited and water resource system is vulnerable across the basin due to the scare and unevenly distributed precipitation over space and time (Zhang et al., 2016a; Wang et al., 2019).

Climate change would certainty complicate the ecosystem and water resource system (e.g., Wu et al., 2015; Luo et al., 2016; Fang et al., 2018a,b; Shang et al., 2019). Many studies have reported that the changes of runoff in the basin are closely related with climate change (Wu et al., 2015; Zhang et al., 2016a,b; Luo et al., 2016; Shang et al., 2019). For example, Luo et al. (2016) found that the climate change contributed 56%, 61% and 93% to runoff changes in the 1980s, 1990s and 2000s for the upper reach of Heihe River basin. Shang et al. (2019) obtained that the climate change contributed 87% of the total runoff changes after 2004. Climate change is also likely to make precipitation distributions more uneven. Wang et al. (2019a,b) projected the future precipitation across the basin and found a dramatic decreasing trend in mean annual precipitation, and an increasing trend in spring precipitation over the next 30 years (2021–2050) compared to the baseline period (1976–2005), which inevitably have great effects on the temporal distributions of water resources in the future. Under future climate scenarios, the risk of water resources shortage and uneven distribution will continue to remain. Assessing the hydrological responses to future climate change is of great importance to make informed decisions to manage water resources and environmental systems to cope with the hydroclimatic variability.

The most common way to investigate the impacts of climate change on runoff is using calibrated hydrological models by comparing the estimates of modelled runoff for the current climate and for a perturbed climate (e.g. Eregno et al., 2013; Ravazzani et al., 2015; Wu et al., 2015; Zhang et al., 2016a; Senent-Aparicio et al., 2017; Shang et al., 2019), which usually offers the most comprehensive and reliable means of capturing the hydroclimatic response to changes within a basin. In practice, however, hydrological models usually require more detailed inputs and involve many parameters to be calibrated, which restrict their applications in many cases, for example in data-scarce basins. Moreover, the results from the modelling studies are likely to be dependent on the hydrological model and calibration criteria used in the studies (Chiew et al., 2006).

As an alternative, climate elasticity method, proposed by Schaake (1990) and further developed by scholars like Sankarasubramanian et al. (2001), Fu et al. (2007) and Wang et al. (2016), is another important approach to quantify the sensitivity of runoff to climate variables. Hasan et al. (2018) summarized three advantages of climate elasticity method in evaluating the hydrological response to climate change, the parsimony of data requirement, limited modelling experience and easily understood the results with different levels of scientific knowledge. And the most important is, this method can produce quite comparable results with many other complex models (e.g. Reis et al., 2013; Yang et al., 2014; Koster, 2015; Liu et al., 2017; Hasan et al., 2018; Shang et al., 2019). Koster (2015) found that the calculated climate elasticity performed even better in assessing the relationship between evapotranspiration and streamflow efficiencies than several land surface models. Reis et al. (2013) showed that estimates of relative changes in runoff over upper Jaguaribe River basin, Brazil, by using climate elasticity method, were very similar with the results obtained from a more traditional approach of statistical downscaling followed by hydrologic modelling.

Among various methods for estimating climate elasticity, the analytical deviation based on Budyko hypothesis is clear in theory and does not depend on a large amount of historical climate and runoff data (Yang and Yang, 2011), and thus has been widely used in the literatures (Reis et al., 2013; Liu et al., 2017; Xing et al., 2018a,b). When using the analytical derivation based on Budyko framework, the most common deduced climate elasticities are to precipitation and to evaporation (Yang et al., 2014; Xing et al., 2018a), due to these two variables just involved in Budyko framework. Climate elasticities to more variables, e.g. precipitation, temperature, wind speed, net radiation and relative humidity, were also calculated and discussed in the previous studies (Yang and Yang, 2011; Liu et al., 2017; Hasan et al., 2018). However, more variables in the total differential equation may bring more assessment errors (Wang et al., 2016), therefore, relatively fewer but more critical variables should be considered in the estimation of climatic elasticity. Temperature is a key indicator of climate change particularly under the background of global warming. Besides, it is well established as one of the GCM outputs with the least uncertainties (Liu et al., 2017). Consequently, the climate elasticities to precipitation and to temperature are deduced in this study.

The projected precipitation and temperature are derived from the outputs of General Circulation Models (GCMs) which is the primary source of providing information on future climate and increasingly being employed to solve or to assess regional/local issues (Xuan et al., 2017; Luo et al., 2018). Many factors, like initial and boundary conditions, parameter and model structure, etc., would lead to the variability across GCM outputs of future climate (Raje and Mujumdar, 2010). Hence, the GCMs are usually to be evaluated to assess their performances in simulating the historical observations (Xuan et al., 2017; Zamani and Berndtsson, 2018). This enables to choose GCMs of higher performance so that the relevant output obtained from the suitable GCMs can be used for further analysis. Entropy weighted TOPSIS method is employed to rank the performances of 18 alternative GCMs in simulating the two climate variables, precipitation and temperature, and delta-change approach is then used to correct the bias of the selected GCM outputs.

The overall objective of this study is to evaluate the changes of projected runoff across the upper reach of Heihe River basin during 2021–2050 and 2051–2080 based on outputs of the selected GCMs under Representative Concentration Pathway 4.5 (RCP4.5) emission scenarios. Specifically, we aim to (1) derive the runoff elasticities to two climate variables, precipitation and temperature, according to the historical runoff data of 1960 to 2014 under Budyko framework and climate elasticity definition, (2) evaluate the performances of 18 alternative GCMs in simulating the historical observations by using the entropy weighted TOPSIS and obtain the projected precipitation and temperature from the selected GCMs in terms of the delta-change method, and (3) project and discuss the runoff responses to climate change across the basin during the future periods by using climate elasticity method.

2. Study area and data description

2.1. Study area

Heihe River basin is located in the northwest of China, covering an area of approximately 143,000km^2, within the range of 97.1°–102.0°E and 37.7°–42.7°N (Fig. 1). It is a typical continental arid climate with an annual mean precipitation of 150 mm, gradually decreasing from the west to the east. The annual mean temperature over the basin is 6–8 °C, increasing from the mountainous to the plain, and the annual mean potential evaporation is very strong with over 1000 mm on average.

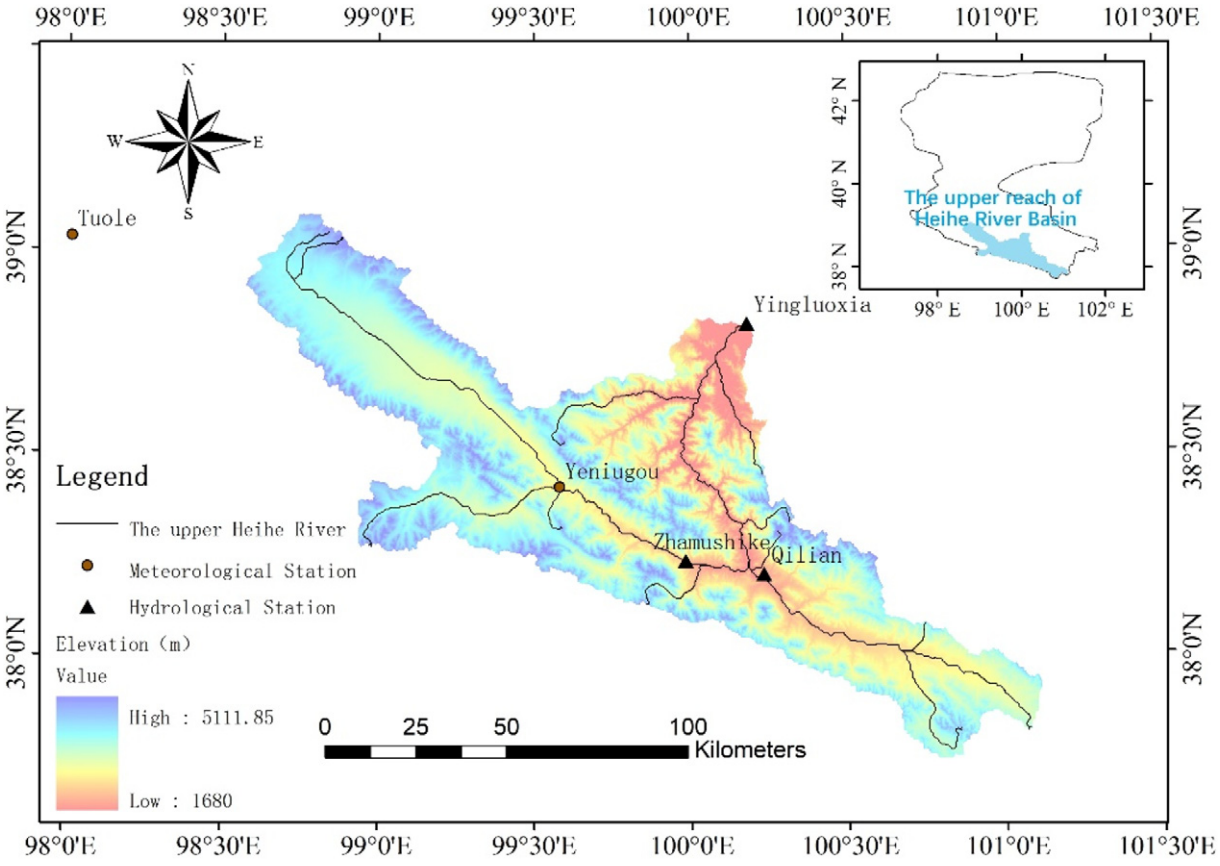

Fig. 1. Locations of Heihe River basin in China and the meteorological and hydrological stations in the upper reach.

The basin can be divided into three parts, the upper, middle and lower reaches. The annual mean precipitation for the upper reach is about 500 mm with unevenly distributed over time. The annual mean temperature is −1 °C or so, and the potential evaporation amounts to about 750 mm. The runoff of the basin mainly comes from the upper reach, which plays a significant role in providing water resources for the whole basin, almost making up the majority of the water available for irrigation, oasis ecosystem, and millions of people living in the middle and lower reaches. Under the background of climate change and human activity, water resource shortage and some problems arising therefrom like grassland degradation and ecological damage have become major factors limiting the sustainable development of the socio-economic and ecological environment over the basin (Shang et al., 2019). Consequently, runoff changes in the upper reach under different scenarios have attracted much attentions from the researchers (Wang et al., 2019; Shang et al., 2019). Here we mainly focus on the effects of future climate change on the long-term runoff since the human influence on the upper reach is comparatively weak (Wu et al., 2015; Zhang et al., 2016b).

2.2. Data description

2.2.1. Climate data

Two kinds of climate data are used to explore the response of runoff to climate change. One is the historical climate data, and the other is the projected climate data from GCMs.

The gridded historical precipitation data used in this study is a regional-scale rainfall product by merging gauge data and regional climate model data, provided by Cold and Arid Regions Science Data Center (http://westdc.westgis.ac.cn) for the period of 1960–2014 with a spatial resolution of 3 km. The historical observations of minimum and maximum temperature, sunshine hour, wind speed and relative humidity are collected from the National Meteorological Information center (http://data.cma.cn) at the two national stations (YNG and QL) for the same period. The data are quality controlled. The information of the national stations can be found in Table 1. These meteorological variables can be used to estimate the potential evapotranspiration at stations.

The future climate projections are derived from 18 alternative GCMs reported in the Coupled Model Intercomparison Project Phase 5 (CMIP5), the detailed descriptions can be seen in Table 2. These GCMs are selected since they were widely applied in climate impact studies with favorable feasibility in China (Xuan et al., 2017; Luo et al., 2018). The GCMs output data are provided by Center for Environment Data Analysis of United Kingdom organization (http://www.ceda.ac.uk). Data for the time slices representing the baseline period of 1960 to 2005, and two long-term projections covering 2021–2050 and 2051–2080 are used. The RCP4.5 (Representative Concentration Pathway 4.5) is considered for the generation of climate change projections as it follows a stabilizing CO_2 concentration close to the median range of all four pathways and will give us a not too extreme indication of what might change.

Table 1
Location information of meteorological and hydrological stations in the study area.

Station name (abbreviation)	Longitude (°)	Latitude (°)	Elevation (m)
Yeniugou (YNG)	38.42	99.58	3180
Qilian (QL)	38.18	100.25	2787
Zhamushike (ZMSK)	38.23	99.98	2810
Yingluoxia (YLX)	38.82	100.18	1700

Table 2
Basic information of the 18 alternative GCMs.

No.	GCM	Time Scale	Resolution (°)	Country
1	ACCESS1–0	Monthly	1.875 × 1.2414	Australia
2	BCC-CSM1.1	Monthly	2.8125 × 2.8125	China
3	BNU-ESM	Monthly	2.8125 × 2.8125	China
4	CanESM2	Monthly	2.8125 × 2.8125	Canada
5	CCSM4	Monthly	1.25 × 0.9375	USA
6	CNRM-CM5	Monthly	1.40625 × 1.40625	France
7	CSIRO-Mk3.6.0	Monthly	1.875 × 1.875	Australia
8	FGOALS-g2	Monthly	2.8125 × 3	China
9	GFDL-CM3	Monthly	2.5 × 2	USA
10	GISS-E2-H	Monthly	2.5 × 2	USA
11	GISS-E2-R	Monthly	2.5 × 2	USA
12	HadGEM2-ES	Monthly	1.875 × 1.2414	England
13	INM-CM4	Monthly	2 × 1.5	Russia
14	IPSL-CM5A-LR	Monthly	3.75 × 1.875	France
15	MIROC5	Monthly	1.40625 × 1.40625	Japan
16	MPI-ESM-LR	Monthly	1.875 × 1.875	Germany
17	MRI-CGCM3	Monthly	1.125 × 1.125	Japan
18	NorESM1-M	Monthly	2.5 × 1.875	Norway

2.2.2. Hydrological data

The observed runoff data at three hydrological stations (QL, ZMSK and YLX, see Table 1) in the study area are used for the analysis. It covers the period of 1960–2014 for ZMSK and YLX stations, and 1967–2014 for QL station. Data of 1988 and 1989 for the three stations are missing and thus interpolated by multi-year average at each station.

3. Method description

3.1. Budyko framework and Zhang's empirical equation

The Budyko framework (Budyko, 1974), describing the long-term water and energy balances of catchments through a curvilinear relationship between the evaporative index and the dryness index, has been widely used in many applications, such as predicting the mean runoff and evaporation over the ungauged basins (e.g. Yao et al., 2017; Shen et al., 2017), assessing the contributions of climate change on runoff changes by the elasticity method (e.g. Yang et al., 2014; Wang et al., 2016), and estimating the contributions of human influence by the decomposition method or the elasticity method (e.g. Zhan et al., 2014; Li and Zhou, 2015), etc.

Several empirical equations describing the relationship between evaporative index and dryness index have been proposed under the Budyko framework with being validated in different watersheds, among which the empirical equation proposed by Zhang et al. (2001) has been widely used in such areas as Yiluo River Basin (Liu et al., 2010) and Wuding River Basin in China (Mou et al., 2017) owing to its features of concise and easy-implemented. For convenience, we call Zhang's empirical equation under the Budyko framework as Budyko-Zhang model in the following section. It is expressed as follows:

$$\frac{E}{P}=\frac{1+\omega(E_0/P)}{1+\omega(E_0/P)+(E_0/P)^{-1}} \tag{1}$$

In which ω is the plant-available water coefficient and represents the relative difference in the way plants use soil water for transpiration. Zhang et al. (2001) interpreted this parameter as mainly owing to differences in root zone depth. Larger values of ω tend to promote evapotranspiration. E_0, E, P are watershed-wide estimates of potential evapotranspiration (mm), actual evapotranspiration (mm) and precipitation (mm), respectively. E can be either estimated from the remote sensing data which is one of the useful data sources for various research fields (e.g., A et al., 2019; Wang et al., 2019a,b), or from the water balance model over a catchment for a long study period. In the calculation of E_0, many methods are available. With considering the data requirements and the numbers of parameters, the temperature-based Blaney-Criddle (BC) method is employed in this study, in which only the variable of temperature and two parameters are involved. The relationship between temperature and potential evapotranspiration is as follows:

$$E_O = ka(0.46T + 8.13) \tag{2}$$

where E_O is the potential evapotranspiration (mm), T is the mean air temperature (°C), a is the percentage of daytime hours for the period (daily or monthly) out of total daytime hours of the year. k is the monthly consumptive use coefficient, depending on vegetation type, location and season, and its initial value is set to be 0.85 in this study according to the reference of Tabari et al. (2013b) and then modified by comparing the E_O results calculated from BC and Penman-Monteith (PM) methods. PM method is by far the most recognized among all the related models and suggested by the Food and Agriculture Organization (FAO) of the United States and many researchers (e.g. Amatya et al., 1995; López-Urrea et al., 2006; Tabari et al., 2013a) due to its excellent performances in both arid and humid climates. Whereas, the E_O values from PM method are not directly used in the application of Budyko-Zhang model here, but regarded as the reference values to modify the parameter k in BC model. This is because that on one hand it is very complex to derive the elasticity to temperature through the partial derivative from PM method, and on the other hand, the requirement of extensive data of this method restricts its applications under limited data availability in the future case.

3.2. Climate elasticity method

According to the water balance model over a catchment, $E = P - Q - \Delta S$, where Q is the runoff of the catchment (mm) and ΔS is the changes in storage which can be considered negligible on the multi-annual scale, Eq. (1) can be written as:

$$\frac{P-Q}{P}=\frac{1+\omega(E_0/P)}{1+\omega(E_0/P)+(E_0/P)^{-1}} \tag{3}$$

That is, Q is a function of the variables P and E_0 and the parameter ω. Parameter ω is estimated by using the multi-year average of the entire datasets of P, Q and E_0 according to Eq. (3). The partial derivative of the function Q with respect to the variable P can be used to define the runoff elasticity to precipitation, ε_P, which is expressed as:

$$\varepsilon_P=\frac{\partial Q}{\partial P}=\frac{3\omega x^2+2x+1}{(\omega x^2+x+1)^2} \tag{4}$$

through mathematical deducing processes, where $x=\frac{E_0}{P}$, the ratio of E_0 to P, is recorded as dryness index, reflecting the degree of climate drought. The runoff elasticity to precipitation can reflect the amount of runoff change caused by a unit change in precipitation. Similar to ε_P, the runoff elasticity to potential evapotranspiration, ε_{E0}, is defined as the partial derivative of the function Q with respect to the variable E_0 and expressed as:

$$\varepsilon_{E_0}=\frac{\partial Q}{\partial E_0}=-\frac{2\omega x+1}{(\omega x^2+x+1)^2} \tag{5}$$

Besides the variable of precipitation, temperature is also a key indicator of climate change particularly under the background of global warming (Liu et al., 2017). Consequently, the runoff elasticity to temperature, ε_T, is defined as well. ε_T is the partial derivative of the

function Q with respect to the variable T. In terms of BC equation for calculating E_0, ε_T can be expressed as:

$$\varepsilon_T = \frac{\partial Q}{\partial T} = \frac{\partial Q}{\partial E_0}\frac{\partial E_0}{\partial T} = -0.46ka\frac{2\omega x + 1}{(\omega x^2 + x + 1)^2} \quad (6)$$

In calculating the above three elasticities, the values of P and E_0 are derived on the multi-annual average scale.

3.3. Budyko-Zhang model performance assessment

After determining the value of parameter ω, the annual runoff can be reproduced based on Eq. (3). For assessing the performance of Budyko-Zhang model to reproduce the changes of runoff in the study area, four indicators, the coefficient of determination (R^2), the relative error (RE), mean absolute deviation (MAD) and root mean squared error (RMSE) are then calculated (Xing et al., 2018a). R^2 can interpret the variance in the observed values that is attributable to the variance in the reproduced values. RE refers to the ratio of absolute error caused by the simulation to the observation, which can reflect the credibility of the model. MAD is the average of the absolute value of the deviation between the simulation and the observation. RMSE is the square root of the deviation, measuring the deviation between the simulation and the observation (Wang et al., 2019b). Four indicators can be calculated as:

$$R^2 = \left(\frac{\sum_{i=1}^{n}\left(Q_{oi}-\overline{Q_o}\right)\left(Q_{si}-\overline{Q_s}\right)}{\sqrt{\sum_{i=1}^{n}\left(Q_{oi}-\overline{Q_o}\right)^2}\sqrt{\sum_{i=1}^{n}\left(Q_{si}-\overline{Q_s}\right)^2}}\right)^2 \quad (7)$$

$$RE = \frac{\overline{Q_s}-\overline{Q_o}}{\overline{Q_o}} \quad (8)$$

$$MAD = \frac{\sum_{i=1}^{n}|Q_{si}-Q_{oi}|}{n} \quad (9)$$

$$RMSE = \sqrt{\frac{\sum_{i=1}^{n}(Q_{si}-Q_{oi})^2}{n}} \quad (10)$$

where Q_{oi} and Q_{si} are the observed and simulated runoff from the Budyko-Zhang model for the ith year, $\overline{Q_o}$ and $\overline{Q_s}$ are the mean values of the observed and simulated runoff for n years.

3.4. Entropy weighted TOPSIS and Delta method

The Technique for Order Preference by Similarity to an Ideal Solution (TOPSIS), first developed by Hwang and Yoon (1981), is one of the most used techniques for resolving the multi-objective and multi-indicator decision making problems in previous literatures (e.g. Zamani and Berndtsson, 2018; Tang et al., 2019; Mojtaba et al., 2019). It is based on the principle that the chosen alternative should have the shortest distance from the ideal solution and furthest distance from the anti-ideal solution (Raju and Kumar, 2014). In this study, the TOPSIS method together with the entropy weight is applied to rank the numerous GCMs according their performances in simulating the observed precipitation and temperature. The steps using this technique are as follows:

First, to determine the decision matrix $X = (x_{ij})_{m\times n}$ according to the indicators evaluated. The value for different indicator must be linearly normalized for the purpose of homogenization, and thus the normalized decision matrix $Y = (y_{ij})_{m\times n}$ can be derived based on the following transformation.

$$y_{ij} = \frac{x_{ij} - x_{min(j)}}{x_{max(j)} - x_{min(j)}} \quad (11)$$

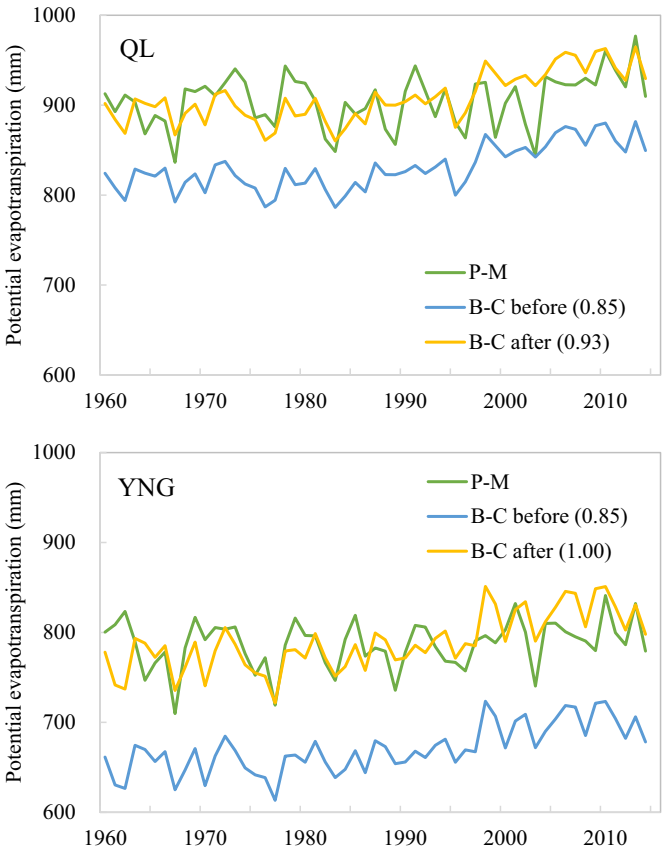

Fig. 2. Comparisons of the estimated E_O values from PM and BC methods (before and after parameter modification).

where x_{ij} means the values of indicator j for the GCMi ($i = 1, 2, 3\ldots$ m, $j = 1, 2, 3\ldots$ n). $x_{max(j)}$ and $x_{min(j)}$ mean the maximum and minimum values of indicator j for all GCMs. The information entropy is employed to determine the weights of each indicator based on the evaluation of the variation degree of each evaluation indicator value, and the weighted normalized decision matrix is $Z = (z_{ij})_{m\times n} = W_j \cdot y_{ij}$, where the entropy-weight of indicator j, W_j, is given by:

$$W_j = \frac{1-H_j}{n-\sum_{j=1}^{n}H_j} \qquad \sum_{j=1}^{n}W_j = 1 \quad (12)$$

$$H_j = \frac{1}{-\ln m}\left(\sum_{i=1}^{m}\frac{\left(1+y_{ij}\right)}{\sum_{i=1}^{m}\left(1+y_{ij}\right)}\ln\frac{\left(1+y_{ij}\right)}{\sum_{i=1}^{m}\left(1+y_{ij}\right)}\right) \quad (13)$$

Second, proximity coefficients, D_i^+ and D_i^-, are calculated in accordance with the ideal value (z_j^*) and anti-ideal values (z_j^{**}) of each

Table 3
Estimations of parameter ω, climate elasticities and the four indicators.

Station		YLX	ZMSK	QL
ω		0.01	0.01	0.07
Indicator	RE	−0.05	−0.08	0.00
	R^2	0.69	0.54	0.55
	RMSE	26.31	36.09	31.12
	MAD	21.90	28.61	23.54
Climate elasticity	ε_P	0.56	0.57	0.56
	ε_{E_0}	−0.12	−0.13	−0.14
	ε_T	−0.016	−0.017	−0.018

indicator for GCM *i*.

$$D_i^+ = \sqrt{\sum_{j=1}^{n}\left(z_j - z_j^*\right)^2} \quad (14)$$

$$D_i^- = \sqrt{\sum_{j=1}^{n}\left(z_j - z_j^{**}\right)^2} \quad (15)$$

This technique is designed to minimize the distance of a data object from the positive ideal solution (D_i^+) and maximise the distance from the negative ideal solution (D_i^-). The relative closeness coefficient (C_i) of each alternative GCM is calculated as:

$$C_i = \frac{D_i^-}{D_i^+ + D_i^-} \quad (16)$$

The performances of GCMs can be ranked according to the values of their closeness coefficient. The larger value of C_i, the better performance of the GCM. Clear examples of TOPSIS approach for ranking GCMs can be found in Raju and Kumar (2014).

In this study, eighteen GCMs are assessed by their performances in simulating two climate variables, precipitation and temperature. Six indicators, namely, mean value (Mean), normalized root mean square error (NRMSE), coefficient of variation (CV), Zc statistic value in Mann-Kendall trend analysis (Zc), coefficient of inhomogeneity (CL) and Pearson correlation coefficient (r) are used for evaluating the performances of GCMs.

Although GCMs are the most advanced numerical tools for deriving the projected climate, the great biases in GCM outputs due to the limited spatial resolution, simplified physics and thermodynamic processes, numerical schemes or incomplete knowledge of climate system processes, restrict their direct applications in many studies on regional or catchment scales (Fronzek and Carter, 2007; Xu and Yang, 2015). Hence, it is important to bias-correct the raw GCM outputs in order to produce climate projections that are better fit for hydrological and the related analysis (e.g. Grillakis et al., 2013; Xu and Yang, 2015). The delta-change approach is one of the methods to correct the bias of GCM outputs (Fronzek and Carter, 2007; Miao et al., 2016). This method is based on the use of a change factor, the ratio between a mean value in the future and historical periods. This factor is then applied to the

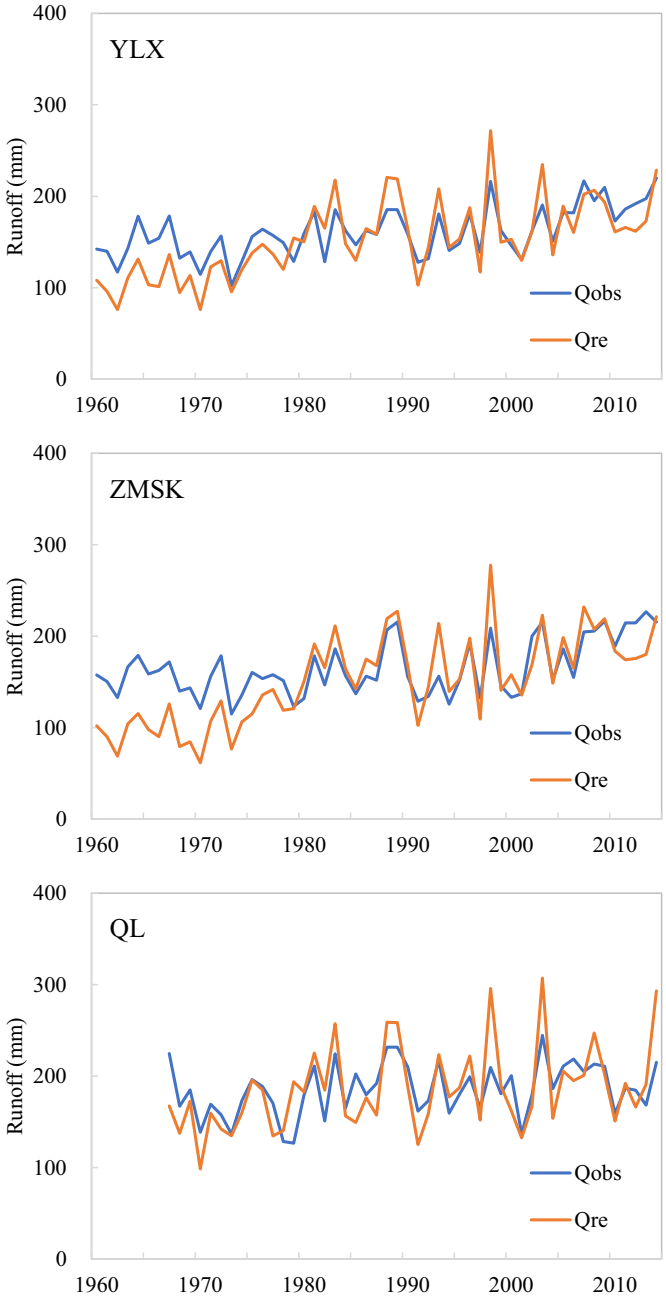

Fig. 3. Comparisons of the observed (blue line) and the reproduced (orange line) runoff based on Zhang's empirical equation under Budyko framework over the study area.

Table 4
Classifications of land use types in different periods over the study area.

Classification I	Classification II	1990	1995	2000	2005	2010	2015
Grass land	High-covered grass land (km^2)	2318	2311	2321	2321	2321	2438
	Middle-covered grass land (km^2)	1531	1547	1531	1531	1531	1589
	Low-covered grass land (km^2)	1155	1139	1204	1204	1204	1260
	Subtotal (km^2)	5004	4997	5056	5056	5056	5287
	Subtotal (%)	50.5	50.6	51.0	51.0	51.0	50.7
Forest land	Shrub forest (km^2)	1164	1167	1164	1164	1164	1261
	Woodland (km^2)	657	668	657	657	657	685
	Sparse woodland (km^2)	251	249	253	253	253	270
	Subtotal (km^2)	2072	2084	2074	2074	2074	2216
	Subtotal (%)	20.9	21.1	20.9	20.9	20.9	21. 2
Waters	Permanent glacier and snow (km^2)	238	262	84	84	80	67
	Bottomland (km^2)	175	176	175	175	175	195
	Rivers and channels (km^2)	6	2	6	6	6	5
	Reservoir and ponds (km^2)	/	/	/	/	/	2
	Subtotal (km^2)	419	440	265	265	261	269
	Subtotal (%)	4.2	4.5	2.7	2.7	2.6	2.6
Crop land	Dry land (km^2)	27	27	27	27	27	28
	Paddy field (km^2)	/	1	/	/	/	/
	Subtotal (km^2)	27	28	27	27	27	28
	Subtotal (%)	0.3	0.3	0.3	0.3	0.3	0.3
Building land	Rural land (km^2)	6	10	6	6	6	8
	Urban land (km^2)	3	2	3	3	3	3
	Subtotal (km^2)	9	12	9	9	9	11
	Subtotal (%)	0.1	0.1	0.1	0.1	0.1	0.1
Unused land	Rock land (km^2)	585	618	640	640	644	685
	Swamp land (km^2)	468	589	468	468	468	489
	Sandy land (km^2)	35	43	35	35	35	35
	Bare land (km^2)	43	45	43	43	43	50
	Gobi Desert (km^2)	2	1	2	2	2	3
	Others (km^2)	1244	1028	1289	1289	1289	1362
	Subtotal (km^2)	2377	2324	2477	2477	2481	2624
	Subtotal (%)	24.0	23.5	25.0	25.0	25.0	25.1

observed time series to transform this series set into time series that is representative of the future climate (Hay et al., 2000; Miao et al., 2016). In this study, the period of 1961–1990 is assumed to be as the baseline period, and the observed data for the baseline period are applied to obtain the two 30-year future climate scenarios for the period of 2021–2050 and 2051–2080. Note that, the change factors for precipitation and temperature are different. The future precipitation and temperature are estimated as follows according the delta-change method.

$$P_f = P_o \frac{\overline{P_f}}{\overline{P_b}} \tag{17}$$

$$T_f = T_o + (\overline{T_f} - \overline{T_b}) \tag{18}$$

where P_f and T_f are the adjusted future precipitation and temperature, P_o and T_o are the observed precipitation and temperature for the baseline period (1961–1990), $\overline{P_f}$, $\overline{T_f}$, $\overline{P_b}$, $\overline{T_b}$ are the monthly mean precipitation and temperature for the future (2021–2050 and 2051–2080) and the baseline periods from GCMs.

4. Results and discussion

4.1. Estimations of parameter ω and climate elasticity

The E_O values should be calculated before estimating the parameter ω. The blue line in Fig. 2 shows the calculated E_O curves by using BC method with the initial value of parameter k, and the green line shows the curves by using PM method. Clearly, BC method tends to underestimate the E_O as a whole. After modifying the parameter value, the two curves are closer. Then the E_O values based on BC method with modified parameter k at QL and YNG stations, and their arithmetic mean will be used to estimate the parameter ω through Eq. (3) according to water balance model over the basin.

Table 3 illustrates the value of parameter ω, together with the four indicator estimates (R^2, RE, RSME and MAD). Overall, R^2 ranges from 0.54 to 0.69, indicating that the calculated runoff based on Budyko-Zhang model can explain about 54–69% of variations in the observed runoff. Fig. 3 shows the observed and reproduced runoff with ω being 0.01, 0.01 and 0.07 for the three stations. As shown, the changes of the two runoff curves coincide largely as a whole, indicating that Budyko-Zhang model has good performance in reproducing the runoff series over the study area.

Many literatures discussed the relationships between the parameters in Budyko-type models (The common formulas for the Budyko hypothesis are called Budyko-type models here) and the influencing factors like climatic seasonality (e.g., drought index, average storm depth, etc.), catchment characteristics (e.g., soil properties, topography, vegetation, catchment slope, etc.), agricultural activity (e.g., cultivation and irrigation), etc., and concluded that many of the factors contribute the changes of parameter in Budyko-type model (e.g., Yang et al., 2014; Jiang et al., 2015; Xing et al., 2018b). Yang et al. (2014) found that the parameter in one Budyko-type model has a logarithmic relationship with catchment slope. Xing et al. (2018b) found that, besides the influencing factors, the interactions between the factors can also affect the parameter estimations. Understanding and quantifying such

Table 5
The original and the normalized indicators for evaluating the performances of 18 GCMs in precipitation and temperature simulation over the study area.

No.	GCMs		Precipitation						Temperature					
			Mean (mm)	C_V	Zc	C_L	NRMSE	r	Mean (°C)	C_V	Zc	C_L	NRMSE	r
1	CCESS1.0	①	17.8	0.33	1.37	0.14	0.94	0.27	3.1	12.93	0.79	0.00	0.42	0.02
		②	0.4	0.59	0.43	0.38	0.27	0.26	0.6	0.02	0.15	0.21	0.57	0.36
2	BCC-CSM1.1	①	16.9	0.45	0.26	0.25	0.96	0.36	2.4	17.64	0.77	0.00	0.32	0.02
		②	0.3	0.83	0.00	0.88	0.29	0.50	0.4	0.03	0.14	0.05	0.29	0.09
3	BNU-ESM	①	46.8	0.54	2.87	0.28	1.76	0.39	1.7	50.12	0.47	0.00	0.32	0.02
		②	1.0	1.00	1.00	1.00	1.00	0.58	0.3	0.09	0.05	0.35	0.29	0.24
4	CanESM2	①	20.9	0.08	0.50	0.06	1.11	0.16	0.8	1.30	0.95	0.00	0.36	0.02
		②	0.4	0.09	0.09	0.00	0.42	0.00	0.1	0.00	0.20	0.69	0.41	0.34
5	CCSM4	①	19.2	0.24	0.78	0.13	0.99	0.22	0.4	3.14	1.04	0.00	0.22	0.01
		②	0.4	0.40	0.20	0.33	0.31	0.14	0.0	0.00	0.22	0.25	0.00	0.00
6	CNRM-CM5	①	25.4	0.10	1.59	0.09	1.27	0.18	3.6	4.27	3.43	0.00	0.49	0.02
		②	0.5	0.14	0.51	0.15	0.57	0.04	0.7	0.01	0.95	0.56	0.76	0.30
7	CSIRO-Mk3.6.0	①	9.2	0.03	1.71	0.06	0.77	0.18	0.3	2.86	1.36	0.00	0.23	0.02
		②	0.2	0.00	0.55	0.00	0.12	0.04	0.0	0.00	0.32	0.20	0.04	0.14
8	FGOALS-g2	①	10.2	0.48	0.35	0.24	0.91	0.46	0.7	8.64	0.43	0.00	0.29	0.02
		②	0.2	0.89	0.03	0.83	0.24	0.74	0.1	0.01	0.04	0.39	0.21	0.33
9	GFDL-CM3	①	16.4	0.35	1.62	0.20	0.88	0.25	2.4	18.25	1.00	0.00	0.36	0.02
		②	0.3	0.62	0.52	0.64	0.22	0.23	0.4	0.03	0.21	0.25	0.42	0.35
10	GISS-E2-H	①	29.3	0.38	1.42	0.21	1.27	0.29	1.4	55.07	3.60	0.00	0.36	0.04
		②	0.6	0.69	0.44	0.70	0.56	0.33	0.2	1.00	1.00	0.67	0.40	1.00
11	GISS-E2-R	①	18.7	0.50	0.57	0.27	1.14	0.56	2.8	11.16	0.36	0.01	0.47	0.03
		②	0.4	0.92	0.12	0.97	0.45	1.00	0.5	0.02	0.02	1.00	0.72	0.52
12	HadGEM2-ES	①	16.2	0.28	1.48	0.12	0.93	0.27	3.7	11.40	2.39	0.00	0.48	0.02
		②	0.3	0.50	0.47	0.28	0.26	0.28	0.7	0.02	0.63	0.37	0.75	0.14
13	INMCM4	①	26.1	0.43	1.59	0.20	1.25	0.42	3.1	4.20	0.36	0.00	0.42	0.03
		②	0.6	0.79	0.51	0.67	0.55	0.65	0.6	0.01	0.02	0.30	0.58	0.58
14	IPSL-CM5A-LR	①	2.5	0.49	0.48	0.26	0.81	0.42	1.8	3.45	0.71	0.00	0.32	0.03
		②	0.0	0.90	0.08	0.91	0.16	0.66	0.3	0.00	0.12	0.00	0.30	0.90
15	MIROC5	①	28.2	0.29	0.80	0.14	1.21	0.20	5.0	9.40	1.12	0.00	0.57	0.02
		②	0.6	0.52	0.21	0.38	0.51	0.10	1.0	0.02	0.25	0.13	1.00	0.11
16	MPI-ESM-LR	①	18.1	0.23	0.61	0.15	0.99	0.24	2.9	12.56	0.30	0.00	0.36	0.02
		②	0.4	0.38	0.13	0.44	0.32	0.21	0.5	0.02	0.00	0.16	0.41	0.20
17	MRI-CGCM3	①	1.2	0.17	1.66	0.10	0.64	0.23	1.8	2.99	0.67	0.00	0.36	0.02
		②	0.0	0.27	0.53	0.22	0.00	0.17	0.3	0.00	0.11	0.68	0.41	0.20
18	NorESM1-M	①	7.6	0.28	0.80	0.18	0.81	0.33	3.9	11.67	0.30	0.00	0.55	0.02
		②	0.1	0.50	0.21	0.58	0.16	0.43	0.8	0.02	0.00	0.89	0.94	0.04
Weight			0.06	0.08	0.08	0.10	0.06	0.09	0.08	0.08	0.12	0.09	0.08	0.09

Note: ①and ② correspond the original and the normalized values for each indicator.

relationship between model parameters and the influencing factors is a very significant issue since it is helpful in making transparent estimates of changes in either evaporation or runoff under various scenarios. To construct such a relationship, the parameter value in Budyko-type model estimated from long-term observed datasets of P, Q and E_0 is usually assumed as the reference value, and either the spatial or the temporal (or the both) information about the influencing factors are always required. In this study, data available are too scare to make any further investigation in constructing such a relationship, and moreover, we merely focus on the changes of runoff owing to the future climate change with assuming the model parameter value as stable.

For Budyko-Zhang model, the parameter ω is related with the land cover type according to Zhang et al. (2001), the proposer of this empirical equation. Table 4 displays us the land cover and land use types in different periods of 1960–2015 over the study area (http://data.cma.cn/). There are six classifications of land use types, in which grassland area occupying the largest with over 50% of the total area, followed by unused land (including Rock land, Swamp land, Bare land, Sandy land, Gobi Desert, etc., in details) and forest land. Crop land and building land areas are less, being less than 1%. The areas and the corresponding area percentage basically keep stable during the past years for most types of land use except for the waters, that is, all the plant types and areas remain stable. Therefore, it is reasonable to assume the value of parameter ω fixed at the temporal scale in this study with being 0.01, 0.01 and 0.07 for YLX, ZMSK and QL stations, respectively.

Based on the ω value, the climate elasticity is then estimated according to Eqs. (4)–(6), as shown in Table 3. The runoff elasticities to precipitation for YLX, ZMSK and QL stations are positive and quite close from each other, being 0.56, 0.57 and 0.56, respectively, indicating that the increase of precipitation has a positive effect to the runoff increase, and 1 unit (or 10%) increase in precipitation would lead to 0.56–0.57 units (or 5.6–5.7%) increase in runoff over the study area. The runoff elasticity to potential evapotranspiration ranges from −0.12 to −0.14, and the increase of potential evapotranspiration has a negative effect to the runoff increase, 10% increase of potential evapotranspiration results in 1.2–1.4% decrease in runoff. The runoff elasticity to temperature is about −0.02 for all stations, and the negative elasticity means that the temperature increases would lead to the runoff decreases.

Some literatures have documented the runoff elasticity to precipitation over basins in China, with the estimations of 2.6 for Luan River basin (Xu et al., 2013), 1.7–3.3 for Hai River basin (Xu et al., 2014), 1.1 to 1.5 for Southern China and part of the Northwest, 1.6 to 2.0 for the majority of Northwest China and Songhua River basin (Yang et al., 2014). Investigations of runoff elasticity to temperature are relatively scare due to the complexity in deriving and solving the partial differential equations. Among the present studies, it is estimated to be −0.05 for Futuo River catchment in Hai River basin (Yang and Yang, 2011), −0.35 for tropical region, −0.88 for arid region and −0.99 for semiarid region in Nile River Basin (Hasan et al., 2018). For comparisons, a little lower runoff elasticities are obtained from this study. Such differences are possibly related with the climate conditions of the study area, catchment characteristics, the selection of different Budyko-type models and also the datasets used. Especially, the low elasticity to temperature deduced is probably related with the catchment characteristics. As known, the snow and glarier melting and the frozen soil degradation have great influences on river runoff over Heihe River basin. Increased temperature not only enhances the evapotranspiration over the basin, leading to runoff decreasing, but also affects the snow and glacier melting and frozen soil thawing, leading to runoff increasing conversely. The opposite interactions partly make the runoff elasticity to temperature small over the study area.

4.2. Future climate variables derived from the GCMs

Table 5 gives the original and the normalized indicators in TOPSIS for evaluating the performances of 18 GCMs in simulating precipitation and temperature over the study area according to Eqs. (11)–(16). The indicator value obtained from the historical observed series is assigned as the positive ideal solution, and that from the alternative GCM with the maximum distance to the positive ideal solution is assigned to the negative ideal solution. The weight of each indicator based on the entropy weighted approach is determined and shown in the last row of Table 5. Table 6 presents the D_i^+, D_i^-, C_i, along with the ranking pattern for the 18 GCMs. The larger value of C_i, the better performance of the GCM. Clearly, CSIRO-Mk3.6.0, CCSM4, and CanESM2 rank the first three with C_i values of 0.805, 0.782 and 0.734, respectively, and GISS-E2-H, GISS-E2-R and BNU-ESM rank the last three with C_i values of 0.369, 0.467, 0.493. It is suggested that CSIRO-Mk3.6.0, CCSM4, and CanESM2 are more suitable for the study area comparatively. Delta-change method is then applied to these models to correct the projected raw GCM outputs using the differences in the mean and variability between GCM and observations in the baseline period.

Table 6
Ranking patterns of 18 GCMs over the study area based on the entropy weighted TOPSIS method.

No.	GCMs	D_i^+	D_i^-	C_i	Rank
1	ACCESS1.0	0.11	0.20	0.649	6
2	BCC-CSM1.1	0.13	0.21	0.622	8
3	BNU-ESM	0.19	0.18	0.493	16
4	CanESM2	0.09	0.24	0.734	**3**
5	CCSM4	0.07	0.24	0.782	**2**
6	CNRM-CM5	0.16	0.19	0.538	15
7	CSIRO-Mk3.6.0	0.06	0.26	0.805	**1**
8	FGOALS-g2	0.14	0.21	0.605	9
9	GFDL-CM3	0.12	0.20	0.626	7
10	GISS-E2-H	0.21	0.12	0.369	18
11	GISS-E2-R	0.20	0.17	0.467	17
12	HadGEM2-ES	0.14	0.18	0.575	12
13	INMCM4	0.15	0.18	0.540	14
14	IPSL-CM5A-LR	0.16	0.21	0.568	13
15	MIROC5	0.14	0.21	0.596	10
16	MPI-ESM-LR	0.09	0.23	0.721	4
17	MRI-CGCM3	0.09	0.23	0.711	5
18	NorESM1-M	0.15	0.21	0.581	11

Figs. 4 and 5 show precipitation and temperature changes from the GCM outputs after bias correction during the future periods. Compared with the baseline period (1961–1990), all models project higher precipitation in the future periods, increased by approximately 5–16% at the three stations for the first future period (2021–2050), and by 2–22% for the second future period (2051–2080). Whereas, there is a little inconsistency between the three GCMs projections. CISRO-Ck3.6.0 produces most precipitation during the first future period, increased by 9–16% to the baseline period. CanESM2 produces most during the second future period, increased by 11–22%. CCSM4 always projects less

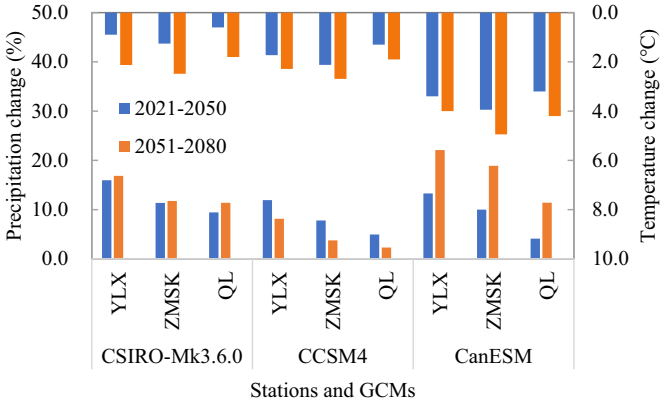

Fig. 4. The projected precipitation and temperature changes derived from the three GCMs during the two future periods over the study area.

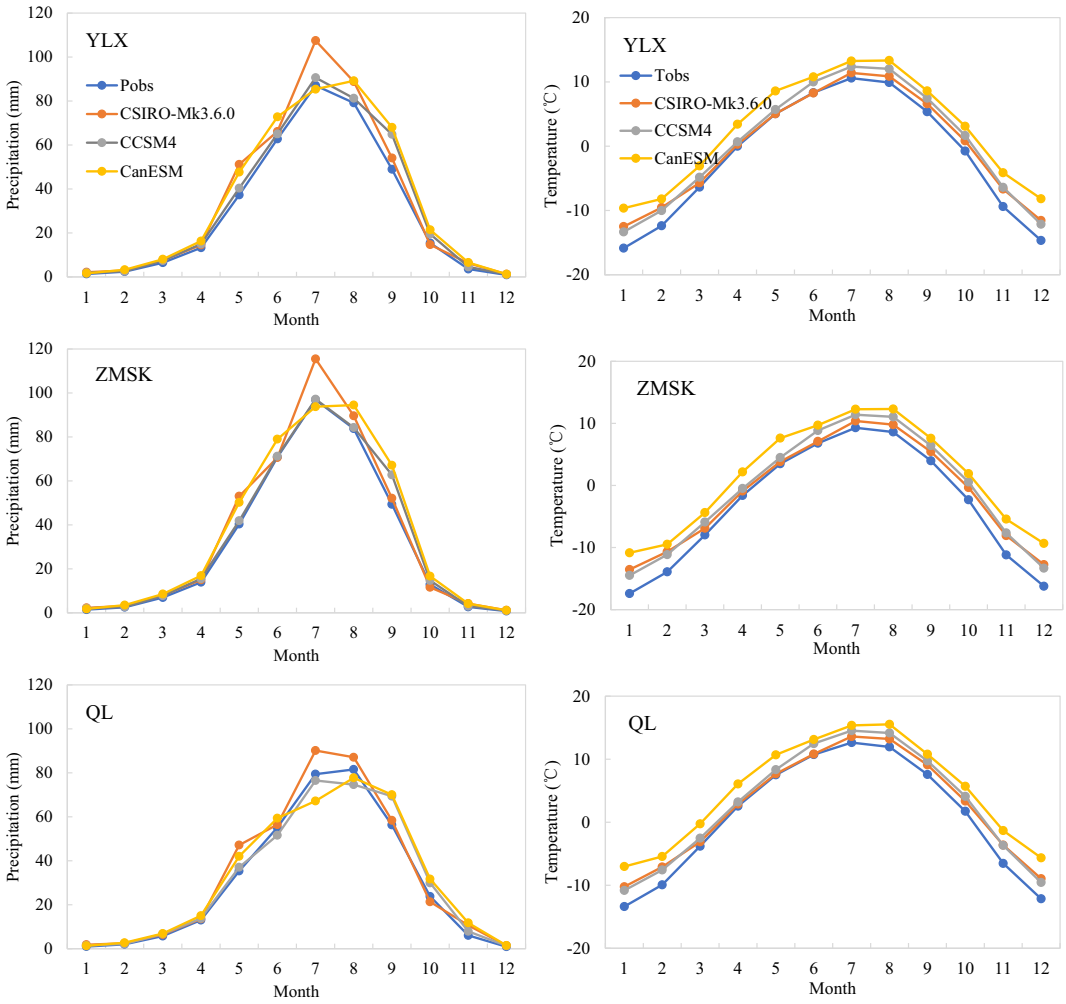

Fig. 5. The observed (1961–1990) and projected (2021–2080) monthly mean precipitation and temperature from GCMs (The blue, orange, grey, yellow lines with dots represent the observations, the projections from CSIRO-Mk3.6.0, CCSM4 and CanESM4, respectively.)

increments in precipitation in the future. Overall, the precipitation projections from the three GCMs increase by 10% on average across the basin during the period of 2021–2050 and by 12% during the period of 2051–2080.

The temperature projections from the GCMs indicate a warmer future climate, with 0.6–3.9 °C increase during the first future period, and 1.8–4.9 °C increase during the second future period for the three stations. On average across the basin, the projected temperatures increase by 2.0 °C and 2.9 °C for the two future periods, respectively. Among the three models, CanESM2 projects highest increases in temperature, followed by CCSM4 and then by CSIRO-Mk3.6.0 for both periods and for all stations.

According to the inner annual distribution of precipitation and temperature from the GCM outputs (see Fig. 5), the precipitation projections from all models keep approximately stable with showing close values relative to the baseline from November to the next April, and display variations from May to October. CSIRO-Mk3.6.0 projects the most Summer precipitation (June to August), and CCSM4 and CanESM4 project the most Autumn precipitation (September to November) with a similar pattern during the two future periods. As to the temperature, CanESM2 projects the temperature rising for all seasons, and the increments are the highest ranging from 3.2–4.9 °C. CCSM4 and CSIRO-Mk3.6.0 project the temperature rising just in Summer, Autumn and Winter seasons, and keep close to the baseline period in Spring.

4.3. Future runoff changes

According to the climate elasticity and the projected climate scenarios, the relative changes in runoff to precipitation and temperature changes can be obtained. Before discussing the results, it is worth noting that, when applying the climate elasticity approach to predict the runoff changes in the future, we assume that the parameter ω reflecting the catchment characteristics is treated as a constant and shows no change from the current stage to the future, although itself may change in the future owing to the changes of land cover and other influencing factors like many literatures stated (e.g., Yang et al., 2014; Xing et al., 2018b). The changes of parameter ω and the resulting effects to the projected runoff are out of the scope of this study. The value of parameter ω is supposed to be stable, and so is the climate elasticity.

Fig. 6 presents the results of the estimated runoff changes in the future periods over the study area. Table 7 illustrates the maximum, minimum and average relative changes of projected precipitation, temperature and runoff. Clearly, the estimated runoff changes are driven by projected precipitation and temperature. Since we suppose the climate elasticity keeping stable, a linear relationship is presented between precipitation change and runoff change with the slope of about 0.6. That is, a 10% precipitation increase leads to a runoff increase of 6% on average (see Fig. 6 and Table 7).

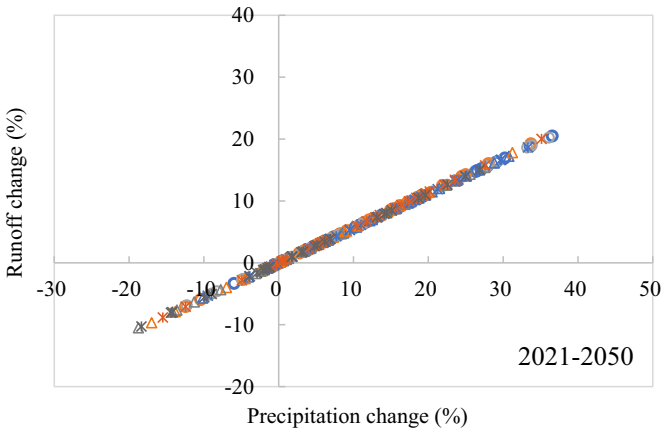

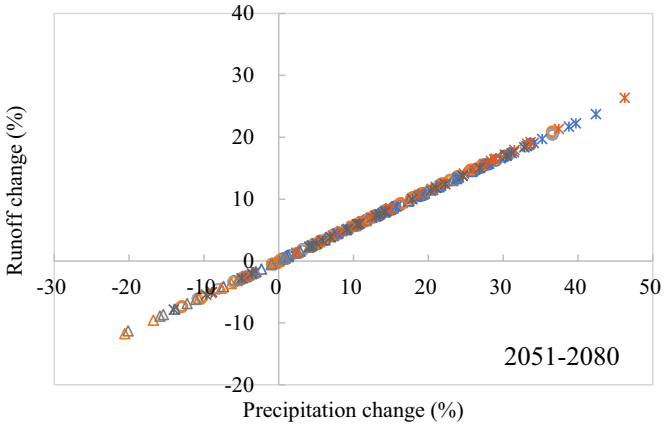

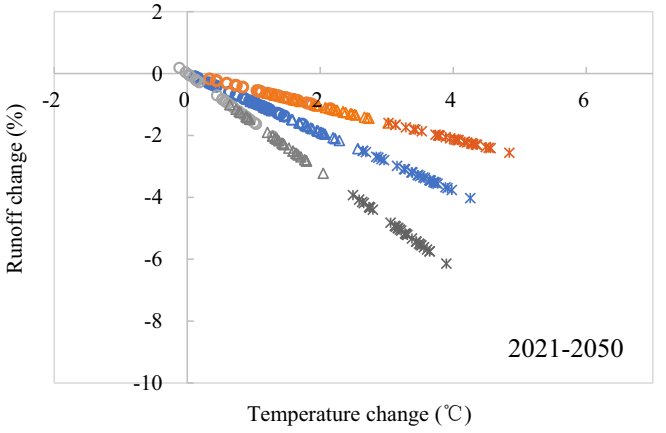

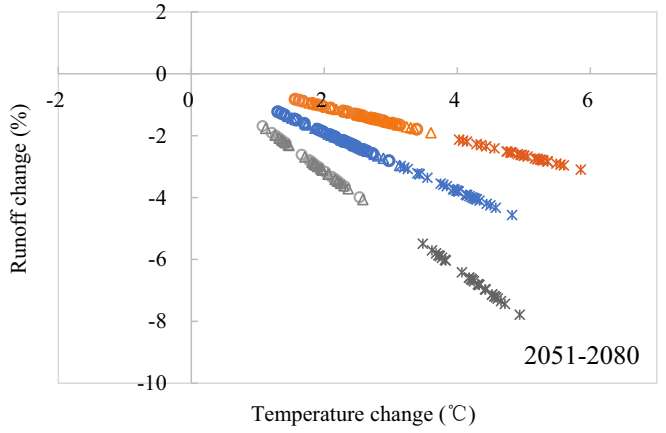

During the first future period (2021–2050), the projected precipitation changes range from −18.8% to 36.6%, leading to the runoff changes ranging from about −10.5% to 20.5%. On average, the relative runoff changes increase by 6.9%, 4.6% and 5.1% from CSIRO-Mk3.6.0, CCSM4 and CanESM2, respectively, in which CSIRO-Mk3.6.0 produces higher runoff not only in the average, but also in the maximum and minimums (see Table 7). During the second future period (2051–2080), higher precipitation changes (more than −20% to approximately 47%) lead to the greater runoff changes, from −11.7% to 26.4%. CSIRO-Mk3.6.0 and CanESM2 result in more than 7.5% and 9.8% runoff increases on average during this period. Overall, due to the effects of precipitation increase, the long-term runoff is projected to increase by 5.6% on average compared with those in baseline period (1961–1990) during the first future period and by 6.7% during the second future period across the study area.

Temperature increase has a negative effect to runoff increase, as shown in Fig. 6. With the projected temperature increasing, the runoff presents decreasing. In details, the runoff during the first future period decreases by 0.8%, 1.6% and 3.5% on average from CSIRO-Mk3.6.0, CCSM4 and CanESM2, respectively, and decreases by 2.1%, 2.2% and 4.4% during the second future period (Table 7). Obviously, CanESM4 leads to greater runoff decreases due to higher temperature projections comparatively in both future periods (see Fig. 6). No matter which GCM is, the projected runoff during the second future period always decreases more than those during the first period owing to the higher projected temperatures. As a whole, with the effects of temperature increase, the long-term runoff is projected to decrease by 2.0% and by 2.9% on average during the first and second future periods compared with those in baseline period (1961–1990).

The estimated runoff changes in Table 7 compare favorably with those obtained from the complex hydrological models. For example, over Heihe River basin, by employing Soil and Water Assessment Tool (SWAT) model, Wu et al. (2015) found that the increases of temperature (increase by +0.8 °C) and precipitation (increase by +10.8%) during 2006–2030 would make the runoff increased by 9.8%, compared to the baseline of 1981–2005. Zhang et al. (2016b) obtained a 4.93% increase in precipitation would lead to 5.17% increase in runoff if only considering the climate change scenario. Shang et al. (2019) estimated that a 10% increase of precipitation would lead to 7.45% increase in runoff. Similarly, Zhang et al. (2016a) concluded that the runoff in Heihe River basin was expected to increase by 11.4% compared to the baseline period (1981–2010) by using improved SWAT model and GCM outputs under scenario RCP4.5. Our results obtained from the more flexible climate elasticity method with the advantage of using fewer data are largely consistent to the reported results in the literatures by using more complicated hydrological models.

It should be noted that, the glarier and snow melting and the frozen soil degradation have great influences on river runoff over Heihe River basin, which has caught lots of attention from the researchers (e.g., Yi et al., 2014; Wang et al., 2015; Li et al., 2016), and some hydrological modelling and new techniques (e.g., Long et al., 2016; Li et al., 2016) were employed in investigating the effects of these factors to runoff changes. The climate elasticity method based on Budyko framework used here does not seem to resolve this issue effectively due to its quite simple and statistic-based model structure with just considering a few climate variables and one model parameter. It inevitably simplifies the hydrological process compared to

Fig. 6. The relative changes of runoff to the changes of precipitation and temperature during the future periods over the study area (The circle, triangle and cross represent the results from CSIRO-Mk3.6.0, CCSM4 and CanESM4, and the blue, orange and grey represent the results of YLX, ZMSK and QL stations, respectively).

Table 7
Relative changes of runoff in the future using the climate elasticity method over the study area.

Period	Value	CSIRO-Mk3.6.0						CCSM4						CanESM2					
		YLX		ZMSK		QL		YLX		ZMSK		QL		YLX		ZMSK		QL	
		ΔP/P	ΔQ/Q	ΔP/P	ΔQ/Q	ΔP/P	ΔQ/Q	ΔP/P	ΔQ/Q	ΔP/P	ΔQ/Q	ΔP/P	ΔQ/Q	ΔP/P	ΔQ/Q	ΔP/P	ΔQ/Q	ΔP/P	ΔQ/Q
2021–2050	MAX	36.6	20.5	33.7	19.2	36.1	20.2	30.8	17.2	31.2	17.8	27.5	15.4	33.3	18.7	35.1	20.0	26.9	15.0
	MIN	−6.0	−3.3	−12.4	−7.1	−12.3	−6.9	−10.2	−5.7	−17.0	−9.7	−18.8	−10.5	−9.5	−5.3	−15.5	−8.8	−18.4	−10.3
	Mean	16.0	8.9	11.4	6.5	9.4	5.3	11.9	6.7	7.8	4.4	5.0	2.8	13.3	7.4	10.0	5.7	4.1	2.3
2051–2080	MAX	36.1	20.2	36.6	20.9	36.5	20.5	25.8	14.5	27.6	15.8	23.3	13.0	42.4	23.7	46.3	26.4	32.8	18.4
	MIN	−4.8	−2.7	−12.9	−7.4	−10.8	−6.1	−13.9	−7.8	−20.6	−11.7	−20.1	−11.3	−3.1	−1.7	−9.0	−5.1	−14.0	−7.8
	Mean	16.8	9.4	11.7	6.7	11.4	6.4	8.1	4.6	3.8	2.1	2.3	1.3	22.1	12.4	18.9	10.8	11.4	6.4
Period	Value	ΔT	ΔQ/Q	ΔT	ΔQ/Q	ΔT	ΔQ/Q	ΔT	ΔQ/Q	ΔT	ΔQ/Q	ΔT	ΔQ/Q	ΔT	ΔQ/Q	ΔT	ΔQ/Q	ΔT	ΔQ/Q
2021–2050	MAX	1.7	−0.1	2.2	−0.2	1.3	0.2	2.6	−0.9	3.0	−0.6	2.0	−1.0	4.3	−2.5	4.8	−1.6	3.9	−3.9
	MIN	0.1	−1.6	0.3	−1.1	−0.1	−2.0	0.9	−2.4	1.2	−1.6	0.6	−3.2	2.6	−4.0	3.0	−2.6	2.5	−6.1
	Mean	0.9	−0.8	1.3	−0.7	0.6	−0.9	1.7	−1.6	2.1	−1.1	1.3	−2.1	3.4	−3.2	3.9	−2.1	3.2	−5.0
2051–2080	MAX	3.0	−1.2	3.4	−0.8	2.5	−1.7	3.1	−1.4	3.6	−0.9	2.6	−1.8	4.8	−3.0	5.9	−2.1	4.9	−5.5
	MIN	1.3	−2.8	1.6	−1.8	1.1	−4.0	1.5	−3.0	1.8	−1.9	1.1	−4.1	3.1	−4.6	4.0	−3.1	3.5	−7.8
	Mean	2.1	−2.0	2.5	−1.3	1.8	−2.9	2.3	−2.2	2.7	−1.4	1.9	−2.9	4.0	−3.8	4.9	−2.6	4.2	−6.7

Note: MAX and MIN mean the maximum and minimum values; Units for ΔQ/Q, ΔP/P and ΔT are %, % and °C, respectively.

those process-based method. Whereas, since all the catchment-related influencing factors like topography, soil properties, the melting of glarier and snow, certainty have effects on runoff generation and flow concertation, the historical observed runoff series used to estimate the parameter in Budyko model are the results of comprehensive effects from multiple factors including both climate conditions and catchment characteristics. That is, the estimated value of parameter in Budyko model can reflect the integrated effects from all influencing factors to some extent, including the glarier and snow melting and frozen soil layer changing. Certainly, for quantifying the contributions of glarier and snow melting and frozen soil degradation to runoff changes, besides the hydrological modelling, to investigate and construct the relationship between these factors and the model parameters under Budyko framework may be a feasible way, as presented in the literatures of Xu et al. (2014), Yang et al. (2014) and Xing et al. (2018b), etc.

As a whole, although in many cases, more accurate estimates on the effects of climate change to runoff for a particular area still need physically based hydrological model, the results here indicate the robust of the simple tool of climate elasticity, which enables to provide a useful overview of the response of long-term runoff to climate change in the study area.

5. Conclusion

This study utilized Budyko-based climate elasticity method, combined with temperature-based Blaney-Criddle equation, to obtain the elasticities of runoff to precipitation and to temperature, and then applied this method to the upper reach of Heihe River basin, China. Then derived the projected climate variable changes from the selected GCMs under RCP4.5 scenario during the two future periods (2021–2050 and 2051–2080) based on the entropy weighted TOPSIS and delta-change method. Finally calculated and discussed the future runoff changes from the projected climate variables with the estimated climate elasticity. The following conclusions were drawn:

1. The runoff elasticity to precipitation in the upper reach of Heihe River basin was estimated to be 0.56–0.57, the elasticities to potential evapotranspiration was −0.12 to −0.14 and to temperature was −0.016 to −0.018.
2. Among the 18 alternative GCMs, CSIRO-Mk3.6.0, CCSM4, and CanESM2 ranked the first three in simulating the historical precipitation and temperature over the upper reach of Heihe River basin according to the entropy weighted TOPSIS method.
3. Relative to the baseline period (1961–1990), the above three GCMs all projected higher precipitation and higher temperature in the future. 10% and 12% increases in precipitation and 2.0 °C and 2.9 °C increases in temperature were projected on average across the basin during the future periods of 2021–2050 and 2051–2080.
4. The long-term runoff was projected to increase by 5.6% and 6.7% with the effects of precipitation increase, and decrease by 2.0% and 2.9% with the effects of temperature increase during the two future periods over the study area.

The value of parameter ω in Zhang's empirical equation under Budyko framework was estimated using the current climate variables including P, E_0, E. We supposed both the parameter ω and the climate elasticity were stable from the current stage to the future in the paper. The limitations for these assumptions may result in the estimated runoff changes uncertain or less than accurate. However, we found that our results with the climate elasticity method were quite comparable with the reported results by using more complicated hydrological models. Therefore, this method with limited hydroclimatic variables is suggested to be applied for many applications especially for those data-scare regions.

Declaration of competing interest

The authors declare that they have no known competing financial interests or personal relationships that could have appeared to influence the work reported in this paper.

Acknowledgements

The first author thanks the financial support by the China Scholarship Council and China University of Geosciences (Beijing), as well as the support provided by CSIRO during her visiting in Australia. This study is supported by the Fundamental Research Funds for the Central Universities (No. 35832015028) and NSFC (No. 41101038).

References

A, Y.L., Wang, G.Q., Liu, T.X., Xue, B.L., Kuczera, G., 2019. Spatial variation of correlations between vertical soil water and evapotranspiration and their controlling factors in a semi-arid region. J. Hydrol. 574, 53–63. https://doi.org/10.1016/j.jhydrol.2019.04.023.

Amatya, D.M., Skaggs, R.W., Gregory, J.D., 1995. Comparison of methods for estimating REF-ET. J. Irrig. Drain. Eng. 121 (6), 427–435. https://doi.org/10.1061/(asce)0733-9437(1995)121:6(427).

Budyko, M.L., 1974. Climate and Life. Acamemic, San Diego.

Chiew, F.H.S., Peel, M.C., Mcmahon, T.A., Siriwardena, L.W., 2006. Precipitation elasticity of streamflow in catchments across the world. Climate Variability & Change Hydrological Impacts. 308.
Eregno, F.E., Xu, C.-Y., Kitterød, N.-O., 2013. Modeling hydrological impacts of climate change in different climatic zones. International Journal of Climate Change Strategies and Management 5 (3), 344–365. https://doi.org/10.1108/IJCCSM-04-2012-0024.
Fang, Q.Q., Wang, G.Q., Liu, T.X., Xue, B.L., A, Y.L., 2018a. Controls of carbon flux in a semi-arid grassland ecosystem experiencing wetland loss: vegetation patterns and environmental variables. Agric. For. Meteorol. 259, 196–210. https://doi.org/10.1016/j.agrformet.2018.05.002.
Fang, Q.Q., Wang, G.Q., Xue, B.L., Liu, T.X., Kiem, A., 2018b. How and to what extent does precipitation on multi-temporal scales and soil moisture at different depths determine carbon flux responses in a water-limited grassland ecosystem? Sci. Total Environ. 635, 1255–1266. https://doi.org/10.1016/j.scitotenv.2018.04.225.
Fronzek, S., Carter, T.R., 2007. Assessing uncertainties in climate change impacts on resource potential for Europe based on projections from RCMs and GCMs. Clim. Chang. 81 (Suppl. 1), 357–371. https://doi.org/10.1007/s10584-006-9214-3.
Fu, G., Charles, S.P., Chiew, F.H.S., 2007. A two-parameter climate elasticity of streamflow index to assess climate change effects on annual streamflow. Water Resour. Res. 43, W11419. https://doi.org/10.1029/2007WR005890.
Grillakis, M.G., Koutroulis, A.G., Tsanis, L.K., 2013. Multisegment statistical bias correction of daily GCM precipitation output. Journal of Geophysical Research Atmospheres 118 (8), 3150–3162. https://doi.org/10.1002/jgrd.50323.
Hasan, E., Tarhule, A., Kirstetter, P., Clark, R., Hong, Y., 2018. Runoff sensitivity to climate change in the Nile River Basin. J. Hydrol. 561 (1), 312–321. https://doi.org/10.1016/j.jhydrol.2018.04.004.
Hay, L.E., Wilby, R.L., Leavesley, G.H., 2000. A comparison of delta change and downscaled GCM scenarios for three mountainous basins in the United States. J. Am. Water Resour. Assoc. 36 (2), 387–397. https://doi.org/10.1111/j.1752-1688.2000.tb04276.x.
Hwang, C.L., Yoon, K., 1981. Multiple Attribute Decision Making. Methods and Applications. Springer, Heidelberg, Germany https://doi.org/10.1007/978-3-642-48318-9.
Jiang, C., Xiong, L., Wang, D., Liu, P., Guo, S., Xu, C.-Y., 2015. Separating the impacts of climate change and human activities on runoff using the Budyko-type equations with time-varying parameters. J. Hydrol. 522, 326–338. https://doi.org/10.1016/j.jhydrol.2014.12.060.
Koster, R., 2015. "Efficiency space": a framework for evaluating joint evaporation and runoff behavior. Bull. Am. Meteorol. Soc. 96 (3), 393–396. https://doi.org/10.1175/BAMS-D-14-00056.1.
Li, J.Z., Zhou, S.H., 2015. Quantifying the contribution of climate- and human-induced runoff decrease in the Luanhe river basin, China. Journal of Water and Climate Change 7 (2), 430–442. https://doi.org/10.2166/wcc.2015.041.
Li, Z.X., Feng, Q., Wang, Q.J., Song, Y., 2016. Contribution from frozen soil meltwater to runoff in an in-land river basin under water scarcity by isotopic tracing in northwestern China. Glob. Planet. Chang. 136, 41–51. https://doi.org/10.1016/j.gloplacha.2015.12.002.
Liu, Q., Yang, Z.F., Cui, B.S., Sun, T., 2010. Temporal trends of hydro-climatic variables and runoff response to climatic variability and vegetation changes in the Yiluo River Basin, China. Hydrol. Process. 23 (21), 3030–3039. https://doi.org/10.1002/hyp.7414.
Liu, J.Y., Zhang, Q., Zhang, Y.Q., Chen, X., Li, J.F., Aryal, S.K., 2017. Deducing climatic elasticity to assess projected climate change impacts on streamflow change across China. Journal of Geophysical Research: Atmospheres 122 (19), 10228–10245. https://doi.org/10.1002/2017JD026701.
Long, Y.P., Zhang, Y.N., Yang, D.W., Luo, L.H., 2016. Implementation and application of a distributed hydrological model using a component-based approach. Environ. Model Softw. 80, 245–258. https://doi.org/10.1016/j.envsoft.2016.03.001.
López-Urrea, R., Martín, S.O.F., Fabeiro, C., Moratalla, A., 2006. Testing evapotranspiration equations using lysimeter observations in a semiarid climate. Agric. Water Manag. 85 (1–2), 15–26. https://doi.org/10.1016/j.agwat.2006.03.014.
Luo, K.S., Tao, F.L., Moiwo, J.P., Xiao, D.P., 2016. Attribution of hydrological change in Heihe River Basin to climate and land use change in the past three decades. Sci. Rep. 6. https://doi.org/10.1038/srep33704.
Luo, M., Liu, T., Amaury, F., Duan, Y.C., Meng, F.H., Bao, A.M., Alishir, K., Philippe, D.M., 2018. Defining spatiotemporal characteristics of climate change trends from downscaled GCMs ensembles: how climate change reacts in Xinjiang, China. Int. J. Climatol. 38 (5), 2538–2553. https://doi.org/10.1002/joc.5425.
Miao, C.Y., Su, L., Sun, Q.H., Duan, Q.Y., 2016. A nonstationary bias-correction technique to remove bias in GCM simulations. Journal of Geophysical Research Atmospheres 121 (100), 5718–5735. https://doi.org/10.1002/2015JD024159.
Mojtaba, H.S., Mohammadkarim, B., Mehdi, R., Ramin, R., 2019. Ranking hospitals based on the disasters preparedness using the TOPSIS technique in Western Iran. Hosp. Top. 97 (6), 1–9. https://doi.org/10.1080/00185868.2018.1556571.
Mou, X., Liu, Q., Ping, F., Liang, J., 2017. Analysis of changes in annual streamflow and its influence factors in Wuding River Basin in the last 50 years (1960–2007). Journal of Beijing Normal University (Natural Science) 53 (4), 465–471. https://doi.org/10.16360/j.cnki.jbnuns.2017.04.015.
Raje, D., Mujumdar, P.P., 2010. Constraining uncertainty in regional hydrologic impacts of climate change: nonstationarity in downscaling. Water Resour. Res. 46, W07543. https://doi.org/10.1029/2009WR008425.
Raju, K.S., Kumar, D.N., 2014. Ranking general circulation models for India using TOPSIS. Journal of Water and Climate Change 6 (2), 288–299. https://doi.org/10.2166/wcc.2014.074.
Ravazzani, G., Barbero, S., Salandin, A., Senatore, A., Mancini, M., 2015. An integrated hydrological model for assessing climate change impacts on water resources of the upper Po river basin. Water Resour. Manag. 29 (4), 1193–1215. https://doi.org/10.1007/s11269-014-0868-8.
Reis, J.D.S., Cerqueira, C.M., Vieira, R.F., Martins, E.S., 2013. Budyko's framework and climate elasticity concept in the estimation of climate change impacts on the long-term mean annual streamflow. World Environmental and Water Resources Congress 2013, 1110–1120. https://doi.org/10.1061/9780784412947.107.
Sankarasubramanian, A., Vogel, R.M., Limbrunner, J.F., 2001. Climate elasticity of streamflow in the United States. Water Resour. Res. 37 (6), 1771–1781. https://doi.org/10.1029/2000WR900330.
Schaake, J.C., 1990. From climate to flow. In: Waggoner, P.E. (Ed.), Climate Change and U.S. Water Resources, pp. 177–206.
Senent-Aparicio, J., Perez-Sanchez, J., Carrillo-Garcia, J., Soto, J., 2017. Using SWAT and fuzzy TOPSIS to assess the impact of climate change in the headwaters of the Segura River Basin (SE Spain). Water 9 (2), 149. https://doi.org/10.3390/w9020149.
Shang, X.X., Jiang, X.H., Jia, R.N., Wei, C., 2019. Land use and climate change effects on surface runoff variations in the upper Heihe River basin. Water 11 (2), 344. https://doi.org/10.3390/w11020344.
Shen, Q.N., Cong, Z.T., Lei, H.M., 2017. Evaluating the impact of climate and underlying surface change on runoff within the Budyko framework: a study across 224 catchments in China. J. Hydrol. 554, 251–262. https://doi.org/10.1016/j.jhydrol.2017.09.023.
Tabari, H., Grismer, M.E., Trajkovic, S., 2013a. Comparative analysis of 31 reference evapotranspiration methods under humid conditions. Irrigation Science Irrigation Science 31 (2), 107–117. https://doi.org/10.1007/s00271-011-0295-z.
Tabari, H., Talaee, P.H., Some'e, B.S., 2013b. Spatial modelling of reference evapotranspiration using adjusted Blaney-Criddle equation in an arid environment. Hydrol. Sci. J. 58 (2), 408–420. https://doi.org/10.1080/02626667.2012.755265.
Tang, J., Zhu, H.L., Liu, Z., Jia, F., Zheng, X.X., 2019. Urban sustainability evaluation under the modified TOPSIS based on grey relational analysis. Int. J. Environ. Res. Public Health 16 (2). https://doi.org/10.1080/10.3390/ijerph16020256.
Wang, Y.H., Yang, D.W., Lei, H.M., Yang, H.B., 2015. Impact of cryosphere hydrological processes on the river runoff in the upper reaches of Heihe River. J. Hydraul. Eng. 46 (9), 1064–1071. https://doi.org/10.13243/j.cnki.slxb.20150001.
Wang, W.G., Zou, S., Shao, Q.X., Xing, W.Q., Chen, X., Jiao, X.Y., Luo, Y.F., Yong, B., Yu, Z.B., 2016. The analytical derivation of multiple elasticities of runoff to climate change and catchment characteristics alteration. J. Hydrol. 541, 1042–1056. https://doi.org/10.1016/j.jhydrol.2016.08.014.
Wang, R.T., Cheng, Q.Y., Liu, L., Yan, C.R., Huang, G.H., 2019. Multi-model projections of climate change in different RCP scenarios in an arid inland region, Northwest China. Water 11 (2), 347. https://doi.org/10.3390/w11020347.
Wang, G.Q., Li, J.W., Sun, W.C., Xue, B.L., A, Y.L., Liu, T.X., 2019a. Non-point source pollution risks in a drinking water protection zone based on remote sensing data embedded within a nutrient budget model. Water Res. 157, 238–246. https://doi.org/10.1016/j.watres.2019.03.070.
Wang, G.Q., Liu, S.M., Liu, T.X., Fu, Z.Y., Yu, J.S., Xue, B.L., 2019b. Modelling above-ground biomass based on vegetation indexes: a modified approach for biomass estimation in semi-arid grasslands. Int. J. Remote Sens. 40 (10), 3835–3854. https://doi.org/10.1080/01431161.2018.1553319.
Wu, F., Zhan, J.Y., Su, H.B., Yan, H.M., Ma, E.J., 2015. Scenario-based impact assessment of land use/cover and climate changes on watershed hydrology in Heihe River basin of Northwest China. Adv. Meteorol. 2015 (2014), 410198. https://doi.org/10.1155/2015/410198.
Xing, W.Q., Wang, W.G., Zou, S., Deng, C., 2018a. Projection of future runoff change using climate elasticity method derived from Budyko framework in major basins across China. Glob. Planet. Chang. 162, 120–135. https://doi.org/10.1016/j.gloplacha.2018.01.006.
Xing, W.Q., Wang, W.G., Shao, Q.X., Yong, B., 2018b. Identification of dominant interactions between climatic seasonality, catchment characteristics and agricultural activities on Budyko-type equation parameter estimation. J. Hydrol. 556, 585–599. https://doi.org/10.1016/j.jhydrol.2017.11.048.
Xu, Z.F., Yang, Z.L., 2015. A new dynamical downscaling approach with GCM bias corrections and spectral nudging. Journal of Geophysical Research Atmospheres 120 (8), 3063–3084. https://doi.org/10.1002/2014JD022958.
Xu, X.Y., Yang, H.B., Yang, D.W., Ma, H., 2013. Assessing the impacts of climate variability and human activities on annual runoff in the Luan River basin, China. Hydrol. Res. 44 (5), 940–952. https://doi.org/10.2166/nh.2013.144.
Xu, X.Y., Yang, D.W., Yang, H.B., Lei, H.M., 2014. Attribution analysis based on the Budyko Hypothesis for detecting the dominant cause of runoff decline in Haihe basin. J. Hydrol. 510, 530–540. https://doi.org/10.1016/j.jhydrol.2013.12.052.
Xuan, W.D., Ma, C., Kang, L.L., Gu, H.T., Pan, S.L., Xu, Y.P., 2017. Evaluating historical simulations of CMIP5 GCMs for key climatic variables in Zhejiang Province, China. Theor. Appl. Climatol. 128 (1–2), 207–222. https://doi.org/10.1007/s00704-015-1704-7.
Yang, H.B., Yang, D.W., 2011. Derivation of climate elasticity of runoff to assess the effects of climate change on annual runoff. Water Resour. Res. 47, W07526. https://doi.org/10.1029/2010WR009287.
Yang, H.B., Qi, J., Xu, X.Y., Yang, D.W., Lv, H.F., 2014. The regional variation in climate elasticity and climate contribution to runoff across China. J. Hydrol. 517, 607–616. https://doi.org/10.1016/j.jhydrol.2014.05.062.
Yao, J.Q., Mao, W.Y., Yang, Q., Xu, X.B., Liu, Z.H., 2017. Annual actual evapotranspiration in inland river catchments of China based on the Budyko framework. Stoch. Env. Res. Risk A. 31 (6), 1409–1421. https://doi.org/10.1007/s00477-016-1271-1.
Yi, J., Zhao, Y., Shao, M.A., Zhang, J.G., Cui, L.L., Si, B.C., 2014. Soil freezing and thawing processes affected by the different landscapes in the middle reaches of Heihe River Basin, Gansu. China. Journal of Hydrology 519, 1328–1338. https://doi.org/10.1016/j.jhydrol.2014.08.042.
Zamani, R., Berndtsson, R., 2018. Evaluation of CMIP5 models for west and southwest Iran using TOPSIS-based method. Theor. Appl. Climatol., 1–11 https://doi.org/10.1007/s00704-018-2616-0.

Zhan, C.S., Zeng, S.D., Jiang, S.S., Wang, H.X., Ye, W., 2014. An integrated approach for partitioning the effect of climate change and human activities on surface runoff. Water Resour. Manag. 28 (11), 3843–3858. https://doi.org/10.1007/s11269-014-0713-0.

Zhang, L., Dawes, W.R., Walker, G.R., 2001. Response of mean annual evapotranspiration to vegetation changes at catchment scale. Water Resour. Res. 37 (3), 701–708. https://doi.org/10.1029/2000wr900325.

Zhang, A.J., Liu, W.B., Yin, Z.L., Fu, G.B., Zheng, C.M., 2016a. How will climate change affect the water availability in the Heihe River Basin, Northwest China? J. Hydrometeorol. 17 (5), 1517–1542. https://doi.org/10.1175/JHM-D-15-0058.1.

Zhang, L., Nan, Z.T., Xu, Y., Li, S., 2016b. Hydrological impacts of land use change and climate variability in the headwater region of the Heihe River Basin, Northwest China. PLoS One 11 (6), e0158394. https://doi.org/10.1371/journal.pone.0158394.

Update

Science of the Total Environment

Volume 766, Issue , 20 April 2021, Page

DOI: https://doi.org/10.1016/j.scitotenv.2020.142628

Science of the Total Environment 766 (2021) 142628

Contents lists available at ScienceDirect

Science of the Total Environment

journal homepage: www.elsevier.com/locate/scitotenv

Corrigendum

Corrigendum to "Impacts of projected climate change on runoff in upper reach of Heihe River basin using climate elasticity method and GCMs" [Sci. Total Environ., 716 (2020) 137072]

Zhanling Li [a,c,*], Qiuju Li [a,c], Jie Wang [a,c], Yaru Feng [a,c], Quanxi Shao [b]

[a] School of Water Resources and Environment, China University of Geosciences (Beijing), Beijing 100083, PR China
[b] CSIRO Data 61, Private Bag 5, Wembley, WA 6913, Australia
[c] MOE Key Laboratory of Groundwater Circulation and Environmental Evolution, China University of Geosciences (Beijing), Beijing 100083, PR China

The authors regret that the printed version of the above article contained an error. The correct and final version follows. The authors would like to apologise for any inconvenience caused.

"5.6% and 6.7% decreases" in the second last sentence of the abstract should be corrected to "5.6% and 6.7% increases".

DOI of original article: https://doi.org/10.1016/j.scitotenv.2020.137072.
* Corresponding author at: School of Water Resources and Environment, China University of Geosciences (Beijing), No. 29 Xueyuanlu Road, Haidian District, Beijing 100083, PR China.
E-mail address: zhanling.li@cugb.edu.cn (Z. Li).

https://doi.org/10.1016/j.scitotenv.2020.142628